Spatial gradient of total electron content (TEC) between two nearby stations as indicator of occurrence of ionospheric irregularity

Teshome Dugassa[1,2], John Bosco Habarulema[3,4], and Melessew Nigussie[5]

[1]Ethiopian Space Science and Technology Institute, Department of Space Science and Application, Addis Ababa, Ethiopia
[2]Bule Hora University, College of Natural and Computational Science, Department of Physics, Bule Hora, Ethiopia
[3]South Africa National Space Agency, Space Science, Hermanus, South Africa
[4]Department of Physics and Electronics, Rhodes University, Grahamstown, South Africa
[5]Washera Geospace and Radar Science Laboratory, Physics Department, Bahir Dar University, Bahir Dar, Ethiopia

Correspondence: Teshome Dugassa (tdugassa2016@gmail.com), John Bosco Habarulema (jhabarulema@sansa.org.za), Melessew Nigussie (melessewnigussie@yahoo.com)

Abstract. The relation between the occurrence of ionospheric irregularity and the spatial gradient of total electron content (TEC) during the post-sunset hours over the equatorial region is studied. Different instruments and techniques have been applied to study the behavior of these ionospheric irregularities. In this study, the Global Positioning System (GPS) based derived TEC was used to investigate the relation between the spatial gradient of TEC between two nearby located stations and the occurrence of ionospheric irregularity over the East Africa longitudinal sector. The gradient of TEC between the two stations (ASAB: 4.34° N, 114.39° E and DEBK: 3.71° N, 109.34° E, geomagnetic) located within the equatorial region of Africa were considered in this study during the year 2014. The rate of change of TEC based derived index ($ROTI$, $ROTI_{ave}$) is also used to observe the relation between the spatial gradient of TEC and the occurrence of ionospheric irregularities. The result obtained shows that most of the maximum enhancement/reduction in the spatial gradient of TEC observed in March and September equinoxes are more pronounced between 19:00 LT - 24:00 LT as the large-scale ionospheric irregularities do. Moreover, the observed spatial gradient of TEC shows two peaks (in March and September) and they exhibit equinoctial asymmetry where the March equinox is greater than September equinox. The maximum enhancement/reduction in the gradient of TEC and $ROTI_{ave}$ during the evening time period also show similar trends but after 1-2 hrs from the equatorial electric field (EEF). The correlation between the spatial gradient of TEC and ROTI show a moderate correlation (C = 0.58 over ASAB, C = 0.53 over DEBK). In addition to latitudinal gradients, the spatial gradient of TEC has a significant contribution on the computation of TEC fluctuation. The spatial gradient of TEC between the two nearby located stations could be used as an indicator of the occurrence of ionospheric irregularities over both stations. The spatial gradient of electron density (TEC) near solar-terminator obtained from two nearby located Global Navigation Satellite System (GNSS) receivers may be used as an alternative method to estimate the strength of the zonal electric field.

Key words: Spatial gradient of TEC, $ROTI_{ave}$, ionospheric irregularities

1 Introduction

The ionosphere, which consists of free electrons and ions, frequently experiences irregular electron density. After sunset, the ionospheric plasma interchange instabilities present in the equatorial/low-latitude ionosphere generate large-scale depletions in the ambient electron density which leads to the formation of plasma density irregularities that affect radio communication and navigation system (Basu and Basu, 1981). The generation of the plasma irregularities can be related to the decrease in plasma production immediately after sunset and the fast recombination rate in the E-region ionosphere, which results in a steep gradient in electron density. The large enhancement of F region vertical plasma drift in the evening hours attests to the presence of enhanced eastward electric field is also another parameter which controls the generation of plasma density irregularities (Fejer, 1991; Fejer et al., 2008). This pre-reversal enhancement (PRE) in the vertical plasma drift moves the F region to higher altitudes (Abdu et al., 2009). When the altitude of F-region is high enough to overcome recombination effects, the Rayleigh-Taylor (R-T) instability mechanisms initiates growth in plasma fluctuations. The R-T instability considered primary responsible for the generation of ionospheric plasma density irregularities or plasma bubbles in equatorial and low-latitude region (Rao et al., 2006a; Fejer et al., 1999). Kelley (2009) reported that the existence of equatorial plasma bubbles (EPB) is attributed to the instability of the R-T plasma which is triggered by the intensification of the eastward equatorial electric field just before its reversal. The characteristics of ionospheric scintillation and ionospheric irregularities over the equatorial and low-latitude region in different longitudinal sectors during different solar and geomagnetic activities has been studied (e.g., Burke et al., 2004; Paznukhov et al., 2012; Oladipo and Schuler, 2013a; Seba and Tsegaye, 2015). From previous work, they have been studied by various instruments such as all-sky imager (Wiens et al., 2006), and very high-frequency radar observation (e.g., Otsuka et al., 2009; Ajith et al., 2016). Recently, GNSS signal analysis is an important tool to study the behavior of ionospheric irregularities (e.g., Pi et al., 1997; Nishioka et al., 2008; Watthanasangmechai et al., 2016; Magdaleno et al., 2017) because of its growing application in civilian and military applications.

The inhomogeneity of ionospheric electron distribution can cause sudden, rapid and irregular fluctuations of the amplitude and phase of the received signals, known as ionospheric scintillation (Wernik and Liu, 1974). As the GNSS signals pass through the ionosphere, the ionospheric irregularities also causes the delay of signals. The inhomogeneity of plasma in the ionosphere might be given as latitudinal (north-south) and longitudinal (east-west) (Jakowski et al., 2004). The spatial plasma density gradients can be represented by means of TEC changes per latitude or longitude (TECU/deg) or by their changes in distance (TECU/km). Radicella et al. (2004) and Nava et al. (2007) also presented the contribution of the horizontal gradients of vertical TEC to positioning error. The characteristics of horizontal ionospheric density gradients and their effects on trans-ionospheric radio wave propagation have been studied at different latitudes (Jakowski et al., 2005; Radicella et al., 2004). Rao et al. (2006a) estimated ionospheric spatial gradient from F-region peak electron density (NmF2) data using a chain of radio soundings. Based on the GNSS data acquired by dense distribution of receivers over Brazilian longitude sector, Cesaroni et al. (2015) highlights the relationship between intensity and variability of TEC gradients and the occurrence of ionospheric scintillation. Previous studies attempts to explain the relation between the latitudinal (N-S) gradient of TEC surrounding the anomaly region and ionospheric scintillation over different sectors (Rao et al., 2006b; Ray et al., 2006; Muella et al., 2008). Recently, Seba

et al. (2018) investigated the relation between equatorial ionization anomaly and night time equatorial spread F (ESF) over East Africa longitudinal sector using data from ground-based GPS stations and a horizontal meridional neutral wind model. However, very few studies have been done over equatorial/low-latitude region of Africa relating the latitudinal/longitudinal gradient of TEC/plasma density and the occurrence of ionospheric irregularities. To identify signals which severely suffer from ionospheric gradient, Ravi Chandra et al. (2009) and Rungraengwajiake et al. (2015) used rate of change of TEC (ROT) and rate of change of TEC index (ROTI). From the definition, however, ROTI mixes both the spatial and temporal gradients of TEC variations. The longitudinal gradient of integrated Pederson conductivity in the E-region at sunset time play a fundamental role in the strengthening the PRE magnitude and affect the generation of ionospheric irregularities (Tsunoda, 1985). It is well known that PRE is a postsunset phenomena which uplift the ionosphere and create a conducive condition for irregularity formation. This implies the magnitude of the zonal electric field is an important parameter for real-time prediction. It is also known that PRE is due to spatial gradient of electron density near solar-terminator. It is not easy to have the longitudinal gradient of electron density over Africa longitude sector as ionosondes are not available in nearby locations as well as study the correlation between the electron density gradient and occurrence of ionospheric irregularities. We know TEC is the integral of electron density, so a closely located GPS receivers would help us to estimate the strength of the zonal electric field and investigate the relation between the gradient of TEC and occurrence of irregularities. It is well known that ROTI is a proxy for occurrence of ionospheric irregularities and scintillations. In this study, the relationship between the spatial gradient of TEC and ROTI were established using ground GPS-TEC receiver from two nearby located stations to observe how gradient of TEC affect radio signals, hence give information that the horizontal electron density gradient as an important parameter to predict ionospheric scintillation. After establishing this relationship showing that both parameters give information about ionospheric irregularities, TEC gradient method may be an alternative as it is a simple computation of establishing the difference. From the study, the contribution of spatial gradient of TEC to ROTI computed from the two GPS-TEC receivers were presented. Moreover, the relation between the daytime eastward equatorial electric field derived from the equatorial electric field (EEF) model and the daytime equatorial electrojet obtained from ground based magnetometer measurements were also discussed. The study is the first of its kind in the African sector to present the relation between the spatial gradient of TEC and occurrence of ionospheric irregularities. This study insight about the possible relation between electric field and irregularities in the postsunset period. The gradients of plasm density might be considered as an important parameter in the modeling of ionospheric irregularities and mitigating positioning errors on GNSS based application.

2 Data and analysis method

The GNSS data used for this study were obtained from University NAVSTAR Consortium (UNVCO) database (http://www.unavco.org/). We used the data from two receiver stations located in the East African region at Debark (Geog. Lat. 13° N, Geog. Long. 37.65° E, Geomag Lat. 4.13° N) and Asab (Geog. Lat. 13° N, Geog. Long. 42.65° E, Geomag. Lat. 4.85° N) for the period 2014. The receiver-independent exchange (RINEX) observation files obtained from the IGS website (http://igscb.jpl.nasa.gov/) were processed by the GPS-TEC application software developed at Boston Collage by Gopi Seemala

(Seemala and Valladares, 2011; Ma and Maruyama, 2003). The TEC analysis software uses the phase and code values for both L1 and L2 GPS frequencies to eliminate the effect of clock errors and tropospheric water vapor to calculate relative values of slant TEC (Sardón and Zarraoa, 1997; Arikan et al., 2008). In order to avoid the multipath effects, different authors have used observation data above certain cutoff mask ranging from 15° to 35° (Chu et al., 2005; Mushini and Pokhotelov, 2011). In the current study, an elevation cutoff mask of 30° was used for all the VTEC computed. Mean vertical TEC (VTEC) values are obtained by averaging the VTEC over 30 min intervals for all satellites in view. Using the computed VTEC collected from the two receiver stations, the spatial gradient of TEC (difference of TEC between two stations per longitudinal separation) was computed for every time and then we analyzed the diurnal, monthly and seasonal variations of the spatial gradient of TEC. The spatial gradient of TEC between the two nearby stations located nearly along the same geographic latitude with longitudinal separation of about $\sim 5^\circ$ or corresponding spatial separation of 535.7 km. Stations with the same latitude were selected to observe only the contribution of the longitudinal gradient to TEC to the probability of occurrence of ionospheric irregularities expressed by ROTI. The spatial gradient of TEC were computed using Eq. (1) (Ravi Chandra et al., 2009; Cesaroni et al., 2015).

$$Spatial\ gradient\ of\ TEC(t) = \frac{VTEC_{asab}(t) - VTEC_{debk}(t)}{\Delta lon} \tag{1}$$

where Δlon represents the difference in the longitude between the two stations. In the analysis of spatial gradient of TEC between the two stations, we applied the absolute value of TEC gradient. Radicella et al. (2004) used the absolute value of gradient of TEC between two stations to explain the effect of horizontal gradient of plasma density to ionospheric delay.

The time variation of TEC also known as rate of change of TEC (ROT) and its derived indices are a good proxy for the phase fluctuation, which is a measure of large-scale ionospheric irregularities (Aarons et al., 1997) were used in this study. These kinds of indices can be used to characterize all the known features of equatorial spread F (ESF) (Mendillo et al., 2000). The rate of change of TEC (ROT) is given by

$$ROT = \frac{TEC_k^i - TEC_{k-1}^i}{t_k^i - t_{k-1}^i} \tag{2}$$

where i is the visible satellite and k is the time of epoch and ROT is in units of TECU/min. The ROTI is defined as the standard deviation of ROT over a 5-min period and mathematically given by Eq. (3) (Pi et al., 1997; Bhattacharyya et al., 2000; Nishioka et al., 2008). Usually, ROTI > 0.5 TECU/min indicates the presence of ionospheric irregularities at scale lengths of a few kilometers (Ma and Maruyama, 2006).

$$ROTI = \sqrt{\langle ROT^2 \rangle - \langle ROT \rangle^2} \tag{3}$$

Oladipo and Schuler (2013b) employed the idea of Mendillo et al. (2000) to obtain a new index called $ROTI_{ave}$ index given in Eq. (4). $ROTI_{ave}$ index is the average of ROTI over 30 min interval for a satellite and then average over all satellites in

view. The index gives average level of irregularities over half an hour. Recently, $ROTI_{ave}$ has been applied to demonstrate and explain the level of ionospheric irregularities over low-latitude/equatorial region of Africa (Oladipo et al., 2014; Bolaji et al., 2019; Dugassa et al., 2019). In this study, the rate TEC fluctuation index (ROTI) and ($ROTI_{ave}$) (Pi et al., 1997; Oladipo and Schuler, 2013b; Oladipo et al., 2014) were used to observe the occurrence of ionospheric irregularities.

$$ROTI_{ave}(0.5hr) = \frac{1}{N}\sum_{n=1}^{N}\sum_{i=1}^{k}\frac{ROTI(n, 0.5hr, i)}{k} \tag{4}$$

where n is the satellite number, $0.5hr$ is half an hour (0, 0.5, 1,... 23.5, 24 UT), i is the 5 min section within half an hour (i = 1, 2, 3, 4, 5, 6), N is the number of satellites observed within half an hour and k is the number of $ROTI$ values available within half an hour for a particular satellite. According to Oladipo and Schuler (2013b), the value of $ROTI_{ave} < 0.4$, $0.4 < ROTI_{ave} < 0.8$ and $ROTI_{ave} > 0.8$, respectively represents the background fluctuation, existence of phase fluctuation, and severe phase fluctuation activities. These threshold values were used to observe the relation between the occurrence of ionospheric irregularities and the spatial gradient of TEC.

The magnetic data used in this study are obtained from International Real-Time Magnetic Observatory Network (INTERMAGNET) and Africa-Meridian B-field Edication and Research (AMBER) installed in Addis Ababa and Adigrat, respectively. It provides one minute values of the northward (X), eastward (Y), vertical (Z) components of the Earth's magnetic field, while horizontal component (H) is computed using Eq. (5).

$$H = \sqrt{X^2 + Y^2} \tag{5}$$

To avoid different offset values of different magnetometers, the nighttime baseline values in the H component (Eq. 6) are first obtained for each day and subtracted from the corresponding magnetometer data sets and obtain the hourly departure of H denoted ΔH expressed by Eq. (7). The baseline value was defined as the average of the H component night time (23:00 - 02:00 LT) value of the Earth's magnetic field.

$$H_o = \frac{H_{23} + H_{24} + H_{01} + H_{02}}{4} \tag{6}$$

where H_{23}, H_{24}, H_{01}, and H_{02} are respectively the hourly values of H at 23:00, 24:00, 01:00 and 02:00 in local time (LT).

$$\Delta H(t) = H(t) - H_o \tag{7}$$

where t is the time in hours ranging from 01:00 to 24:00 LT. The hourly departure ΔH is then corrected for the non-cyclic variation (Eq. 8). This correction was proposed previously Rastogi et al. (2004) and defined non-cyclic variation as a phenomenon in which the value at 01:00 LT is different from that of local midnight (24:00 LT).

$$\Delta c = \frac{\Delta H_{01} - \Delta H_{24}}{23} \tag{8}$$

The hourly departure of H (ΔH) corrected for the non-cyclic variation corresponding to magnetometer data set gives the solar quiet variation (Sq) values as shown in Eq. (9):

$$Sq(t) = \Delta H(t) + (t-1) * \Delta c \tag{9}$$

where t = 1 to 1440. The equatorial electrojet current (EEJ) produces a strong enhancement in the H-component magnetic field measured by magnetometers located within $\pm 5^{\circ}$ of the magnetic equator. Measurements of this magnetic field perturbation in equatorial magnetometers could provide a direct measure of the daytime equatorial electrojet (EEJ) and have strong relationships with dayside vertical velocity ($\boldsymbol{E} \times \boldsymbol{B}$ drift) (Anderson et al., 2004, 2006; Yizengaw et al., 2012). The equatorial stations respond primarily to the EEJ and also to the ring current and the global quiet time Sq current system. However, ground magnetometers just outside the extent of the EEJ ($\sim 6^{\circ} - 9^{\circ}$, off the dip equator) exhibit exact response to the ring and Sq currents, but near-zero response to the EEJ. To obtain the contribution of H-component field to the EEJ current (Eq. 10), we subtract the H-component value recorded at the off the equator ($\sim 6^{\circ} - 9^{\circ}$ geomagnetic) magnetometer from the H-component value measured at the magnetic equator. The subtraction has been made to remove the contribution of the ring current and global Sq dynamo to the H-component. Table 1 gives the list of all the stations for which data has been used in this study.

$$\Delta H = \Delta H_{AAE} - \Delta H_{ETHI} \tag{10}$$

Table 1. Location information and the type of data used in this study.

Name of stations	Code	Geo. lon	Geo. lat	Geom. lon	Geom. lat	Data
Asab, Eritrea	ASAB	42.65° E	13° N	114.34° E	4.85° N	GPS-TEC
Debark, Ethiopia	DEBK	37.65° E	13° N	109.24° E	4.13° N	GPS-TEC
Addis Ababa, Ethiopia	AAE	38.77° E	9.04° N	110.47° E	0.18° N	Magnetometer
Adigrat, Ethiopia	ETHI	39.46° E	14.28° N	111.06° E	5.80° N	Magnetometer

The other data source used in this study is the Real-time model of the Ionospheric Electric Fields (http://geomag.org/models/PPEFM/RealtimeEF.html). The Prompt Penetration Electric Field Model (PPEFM) (Manoj and Maus, 2012) is a transfer

function model which models the daily variations coming from the solar wind, which are mapped in the interplanetary electric field (IEF) data. Eight years IEF data from the ACE satellite, radar data from JULIA, and magnetometer data from the CHAMP satellite were used to derive the transfer function. Using the real-time data from ACE satellite, the transfer function models the current variations in the equatorial ionospheric electric fields. The model takes time and location as input parameters and calculates the best estimates of the equatorial electric field. The model outputs provide the electric field generated as a result of the convective electric field, quiet time electric field, and both. In the present study, we have used only the background quiet-time electric field to observe the relation between the equatorial electric field (EEF) and the spatial gradient of TEC derived from the two nearby stations.

Recently, Nayak et al. (2017) used the real-time model of an electric field to observe the influence of prompt penetration electric field (PPEF) on the occurrence of ionospheric irregularities during 17 March 2015 geomagnetic storm over Indian and Taiwan longitudes. However, this model has not been applied yet to explain the electrodynamic phenomena over African low-latitude region. To use the model in this region, we should first present its relation with equatorial electrojet (EEJ), an indicator of the eastward electric field, during the daytime period over the equatorial region of Africa. To do this, ground-based magnetometer measurements one located at magnetic equator and another one at ($\sim 6^\circ - 9^\circ$) off-equator (Rastogi and Klobuchar, 1990; Anderson et al., 2002; Yizengaw et al., 2014) have been used. Over East Africa longitude, two magnetometer stations, one at Adigrat (ETHI, 14.3° N, 39.5° E, 6.0° N, geomagnetic) and the other at Addis Ababa (AAE, 9.0° N, 38.8° E, 0.2° N, geomagnetic) exists. ETHI and AAE stations belong to AMBER network (Yizengaw and Moldwin, 2009) and INTERMAGNET, respectively. The difference of the H component of the geomagnetic field of the two magnetometer stations, ΔH gives the equatorial electrojet (EEJ) current, which is a proxy to daytime electric field (Anderson et al., 2002; Yizengaw et al., 2014). The relation between the EEF obtained from the real-time electric field model and ΔH were determined. EEF derived from the real-time electric field were used in this study to explain its influence on nighttime enhancement/reduction of the spatial gradient of TEC and the occurrence of ionospheric irregularities. The temporal resolution of EEF and ΔH was 5min and 1 min, respectively. To make their resolution consistent, 5 min average of ΔH of each day were considered. In this study, ΔH derived from the horizontal (H) component of the geomagnetic field of the two stations during quiet days of the year 2012 were used. In this year, we have a large number of magnetometer measurements relative to other years. Monthly five quiet international days of the year 2012 (total of 38) obtained from (http://wdc.kugi.kyoto-u.ac.jp/qddays/index.html) were selected to show the correlation between ΔH and EEF. Since the equatorial electrojet is a day time phenomenon, only the daytime values of EEF and ΔH during (07:00 to 17:00 LT) were considered.

3 Results and Discussions

3.1 Relation between the day-time Equatorial Electrojet (EEJ) and Equatorial Electric Field Model (EEFM)

Figure 1a presents the diurnal variation of EEF and EEJ current signature of H-component of magnetic field on 26 March 2012 and Fig. 1b shows the correlation between the EEJ derived from ΔH and EEF obtained from equatorial electric field

model. The equatorial electric field is a key factor in determining the dynamics and structure of the low-latitude ionosphere (Fejer, 2011). For the first time it was detected by the Jicamarca (11.95° S, 76.87° W) incoherent scatter radar (ISR) and the Jicamarca Unattended Long-Term studies of the Ionosphere and Atmosphere (JULIA) system during the period from 1998 to 2008. However, there were no direct continuous electric field observations from ground-based and when available, mostly limited. Over the African region, there are no ground-based measurements of the zonal electric fields. Anderson et al. (2002) proposed ΔH deduced from ground-based magnetometers as a proxy of equatorial electrojet current. They reported that the vertical plasma drifts observed from Jicamarca ISR has a positive and linear relation with ΔH and henceforth the ΔH was widely taken as a substitution for the EEF. The relation between ΔH derived from H-component of magnetic field observations and EEF obtained from equatorial electric field model for each month five (5) international quiet days of the year 2012 during the daytime (07:00 - 17:00 LT) is shown in Fig. 1b. As illustrated in Fig. 1b, the daytime (07:00 - 17:00 LT) value of ΔH correlate positively and linearly with the quiet-time EEF with correlation coefficient of (C = 0.60). The magnitude and direction of the dayside vertical velocity ($\boldsymbol{E} \times \boldsymbol{B}$ drift) strongly correlates with ΔH (Anderson et al., 2004, 2006; Yizengaw et al., 2011). Studies show that the daytime electrodynamics play a decisive role in the initiation of post-sunset ESF (e.g., Mendillo et al., 2001; Valladares et al., 2001, 2004). The connection between the occurrence of ESF during the evening sector preceded by the rapid rise in F-layer and the strength of EEJ before sunset has been presented (Dabas et al., 2003; Burke et al., 2004; Kelley, 2009; Uemoto et al., 2010; Ram et al., 2007). Sreeja et al. (2009) reported observational evidence for the plausible linkage between the daytime EEJ related electric field variations with the postsunset F-region electrodynamics. Furthermore, Hajra et al. (2012) indicate that the afternoon/evening time variation of the eastward electric field as revealed through EEJ seems to play a dominant role in dictating postsunset resurgence of EIA and consequent generation of spread-F irregularities. Even though ΔH and equatorial electric field derived model (EEF) do not correlate strongly enough over East Africa longitudinal sector, we might use the model derived equatorial electric field over equatorial/low-latitude region of Africa to explain some special features of ionospheric phenomena like plasma density irregularities and the enhancement/reduction of the spatial gradient of TEC between the two stations.

3.2 Relation between the equatorial electric field (EEF), the spatial gradient of TEC and occurrence of ionospheric irregularities

Figure 2a-l show the diurnal variation of the quiet-monthly mean of EEF (along $\sim 40^\circ$ E) and the quiet-monthly mean of the gradient of TEC in the year 2014. The red and blue curve indicate the EEF and the TEC gradient, respectively. The maximum enhancement/reduction in the gradient of TEC and the peak value in the EEF observed during the pre-midnight period was prevalent in the equinoctial months. After the post-sunset period, the maximum enhancement/reduction in the value of the gradient of TEC on solstice months was small compared to equinoctial months. The EEF start rising nearly after 16:00 LT and show enhancement in the evening local time (∼18:00 LT). Most of the maximum enhancement/reduction of the gradient of TEC was observed in the pre-midnight (19:00 - 24:00 LT) and postmidnight (24:00 - 06:00 LT) but after 1-2 hr of the post-sunset enhancement of the equatorial electric field. However, the spatial gradient of TEC observed during the daytime

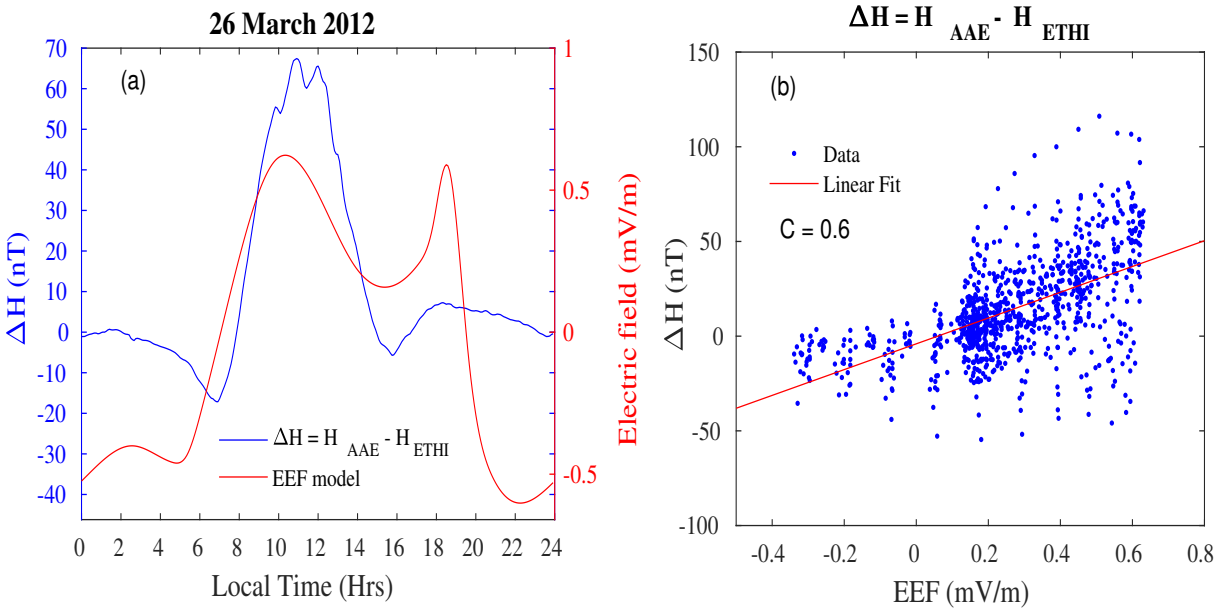

Figure 1. (a) Examples showing the diurnal variation of Equatorial Electric field Model (EEF) (Red panel) and ΔH (blue panel) during 26 March 2012 and (b) The correlation between the equatorial electrojet (EEJ) and quiet-time equatorial electric field model (EEF) during day-time (07:00-17:00 LT) period for quiet days of year 2012. The red line shows the linear fit of data points.

was relatively small compared to the evening time hours for most of the days. The maximum enhancement/reduction in the gradient of TEC observed in the evening period could be related to the pre-reversal enhancement in a zonal electric field.

Figures 3a - d indicate examples showing the diurnal variations of the spatial gradient of TEC and ROTI over ASAB and DEBK stations. The blue, black and the red curves, respectively, indicate the spatial gradient of TEC, and the phase fluctuation index (ROTI) over Asab and Debark. In the post-sunset hours, after 18:00 LT, the pattern of ROTI observed in both stations and the gradient of TEC show a similar trend. The enhancement in the gradient of TEC and the occurrence of irregularities in the post-sunset period could be explained by the presence of ionospheric electrodynamics. The post-sunset period electrodynamics is influenced by F-region dynamo which is governed by a longitudinal gradient of the electrical conductivity and thermospheric zonal wind (Crain et al., 1993). Anderson et al. (2004) showed that the scintillation activity is related to the maximum $E \times B$ drift velocity between 18:30 and 19:00 LT. Mendillo et al. (2001) have pointed out that the best available precursor for pre-midnight ESF is the EIA strength at sunset, which in turn influenced by the magnitude of PRE. Using differential TEC profiles, TEC (at 18:00 hr) - TEC (at 20:00 hr), Valladares et al. (2004) explained that the PRE of the vertical drift would reenergize the fountain effect.

It has been reported that the eastward component of electric field manifested by the vertical plasma drifts over equator and intensified around/shortly after sunset before reversing to westward is one of the most important parameters responsible

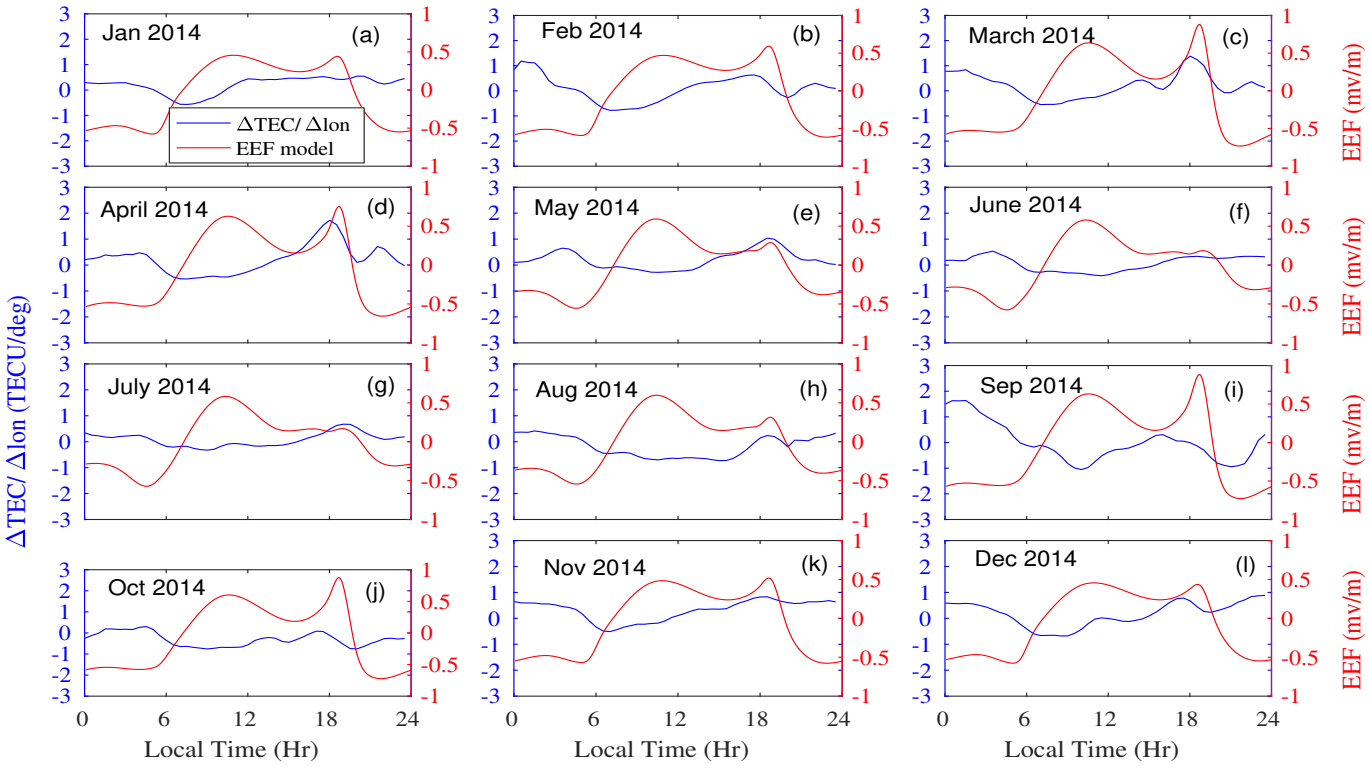

Figure 2. Comparison of Quiet-Monthly Mean of EEF derived from real-time electric field model at about ($\sim 40^{\circ}$ E) and spatial gradient of TEC between ASAB and DEBK in the year 2014.

for driving many interesting ionospheric phenomena, like the Appleton density anomaly and the stability of the nighttime ionosphere (e.g., Horvath and Essex, 2003; Abadi et al., 2015). In the evening sectors, the vertical drift enhancement is of particular significance as it is the major drivers for the generation of ESF (Farley et al., 1970; Woodman, 1970; Basu et al., 1996; Fejer et al., 1999; Martinis et al., 2005). Tulasi Ram et al. (2006) reported that the rapid enhancement of post-sunset of the zonal electric field leads to a large vertical plasma drift ($\boldsymbol{E} \times \boldsymbol{B}$), thereby lifting the F-layer to higher altitudes resulting in a condition conducive for the generation of ESF. Vertical drifts are taken as the key parameters determining the dynamics of ionospheric F-region, and the occurrence of ESF. Ionospheric irregularities are mostly observed over equatorial/low-latitude region an hour or two hours after the PRE. Rastogi and Woodman (1978) showed ESF can appear at any time of the night other than the post-sunset period following the abnormal reversal of the vertical F-region drifts to an upward direction, with a delay of about 1-2 hr. From the figure, the post-sunset enhancement in the zonal electric field as shown in the equatorial electric field model has a profound effect on the enhancement of the spatial gradient of TEC during the post-sunset period. This might indicate that the spatial gradient of TEC as an indicator of the occurrence of ionospheric irregularities. Different researchers used the concept of ionosphere spatial gradient based on multi-GNSS observations within a small scale region to provide corrections and integrity information to the Ground-Based Augmentation System (GBAS) and they attribute the large

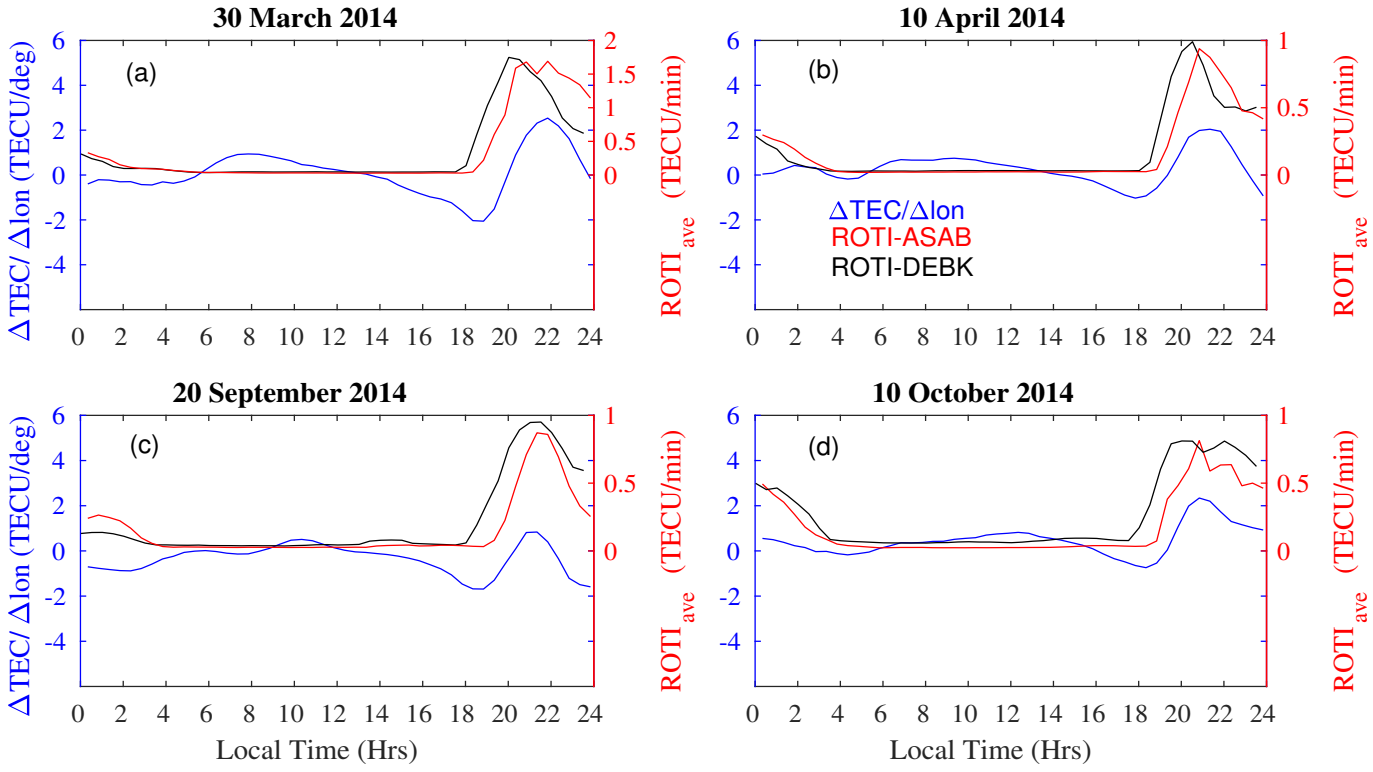

Figure 3. An example showing diurnal variation of the patterns of the spatial gradient of TEC and the ROTI over ASAB and DEBK stations on a) 30 March 2014, b) 10 April 2014, c) 20 September 2014 and b) 10 October 2014.

ionosphere spatial gradient to the TEC enhancements and the ionosphere irregularities (Rungraengwajiake et al., 2015; Saito and Yoshihara, 2017). Saito and Yoshihara (2017) reported that ionosphere gradient can be generated by plasma bubbles.

The patterns of the spatial gradient of TEC and ROTI during geomagnetic storm days were illustrated in Fig. 4a-d. These storm days are categorized as moderate magnetic storms (-100 nT $\leq$ Dst $\leq$-50 nT) (Echer et al., 2013). When the presence of ionospheric irregularities are observed (ROTIave$\geq$ 0.4 TECU/min), the magnitude of spatial gradient of TEC in the post-sunset period is enhanced (during 13 September) and when the presence of ionospheric irregularities are suppressed (ROTIave$\leq$ 0.4 TECU/min), the magnitude of TEC gradient in the nighttime period is reduced (19 February and 27 August). During these seasons, however, the magnitude of TEC gradient shows enhancement in the daytime. Using phase fluctuation index (fp), Kassa and Damtie (2017) reported the inhibition effect of a storm of 19 September on the occurrence of ionospheric irregularities over Ethiopia.

Figures 5a and b show ionospheric irregularity occurrence using the phase fluctuation index ($ROTI_{ave}$) at ASAB and DEBK in the year 2014, respectively. The $ROTI_{ave}$ values are indicated in the color scale. The occurrence of ionospheric irregularities at the two stations, as indicated by $ROTI_{ave}$ value, is a post-sunset phenomenon. The implication of this is that the large-scale

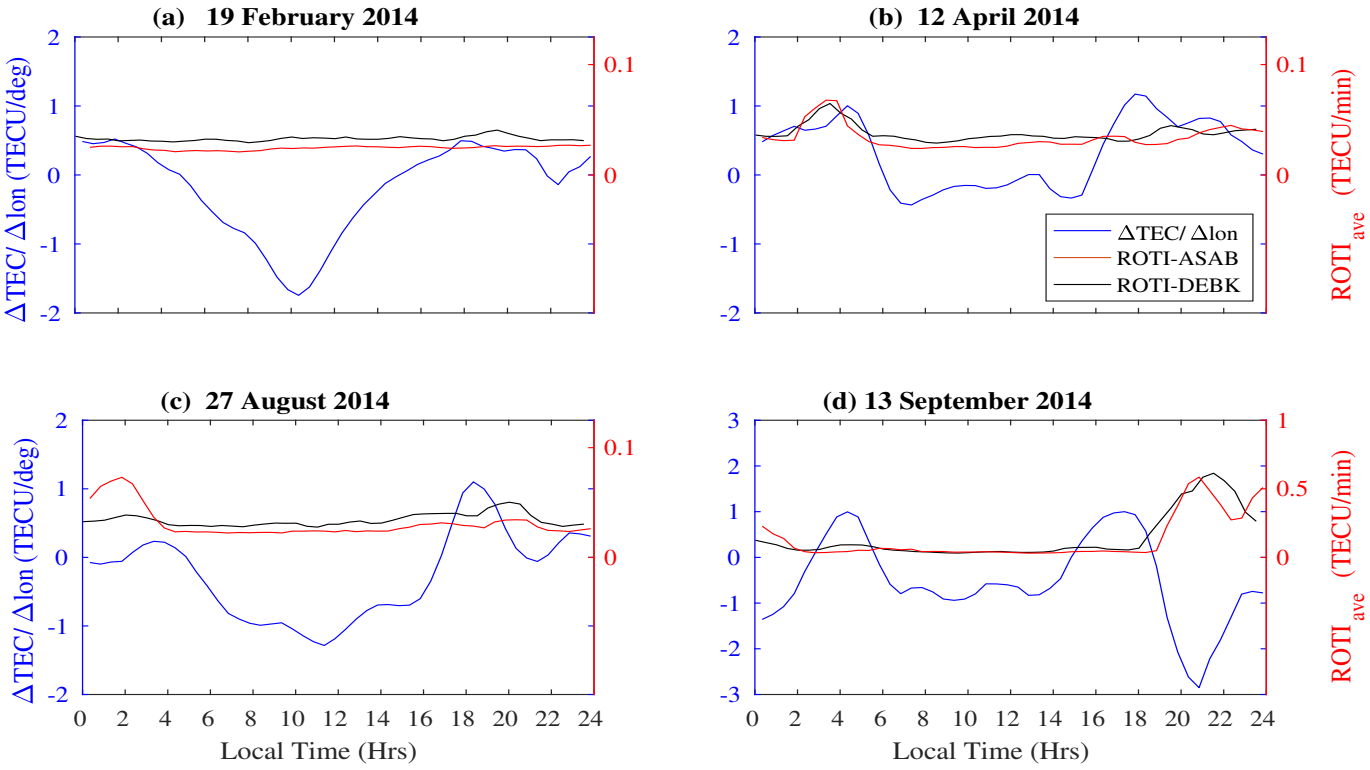

Figure 4. An example showing diurnal variation of the patterns of the spatial gradient of TEC and the ROTI over ASAB and DEBK stations during geomagnetic storm days (a) 19 February 2014 (b) 12 April 2014 (c) 27 August 2014 and (d) 13 September 2014.

ionospheric irregularities, which are responsible for the scintillation of trans-ionospheric signals at GNSS frequencies, are more pronounced during post-sunset hours. The observed phase fluctuation shows monthly variations and there is also a seasonal trend in the occurrence of ionospheric irregularity (see., Fig. 7). Maximum irregularities are observed in March equinox months and minimum in June/July. During this period, the occurrence of phase fluctuation showing irregularities is observed mainly between 19:00 LT and 24:00 LT. As stated by Oladipo and Schuler (2013b), the value of $ROTI_{ave} \geq 0.4$ shows the presence of ionospheric irregularity.

Figure 5c shows the annual variation of the spatial gradient of TEC between DEBK and ASAB in the year 2014. In the computation of the spatial gradient of TEC (using Eq. 1), negative/positive values in the gradient of TEC were observed. The negative/positive values of TEC gradient depends on the value of TEC at the reference station and it denotes an increase/a decrease in the value of TEC gradient. The maximum enhancement and reduction in the value of the gradient of TEC were observed mostly during the post-sunset (18:00 - 24:00 LT) and postmidnight (24:00 - 06:00 LT) period. Equation (1) was applied to all days (364 days) of year 2014 in computing the spatial gradient of TEC. Out of the total observed daily maximum value of the gradient of TEC, about 194 days (in percent about 53 %) of them fall in this time period. There was also a case

where the maximum enhancements and reductions in the value of the gradient of TEC were observed in the early morning period.

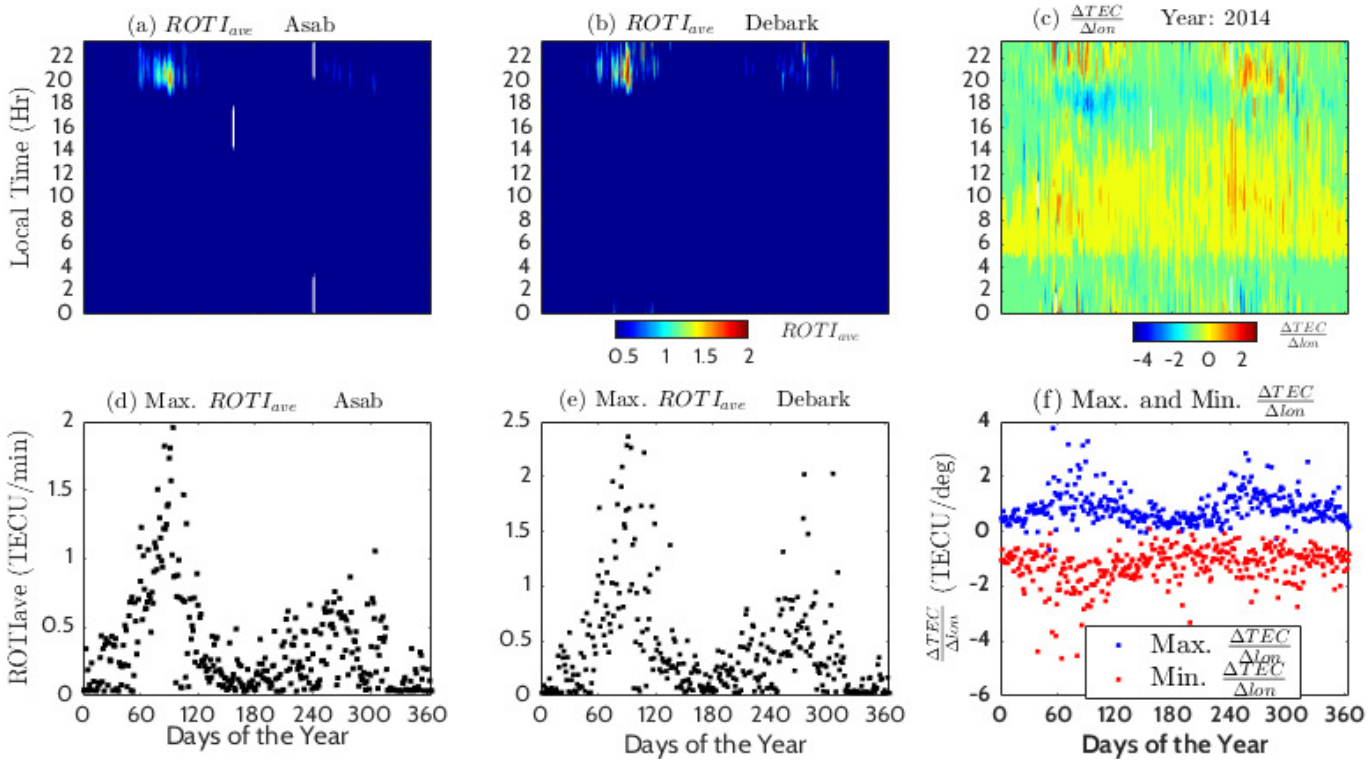

Figure 5. Ionospheric irregularity occurrence at (a) Asab (ASAB), Eritrea (b) Debark (DEBK), Ethiopia. (c) spatial gradient of TEC between ASAB and DEBK, in year 2014. Daily maximum value of $ROTI_{ave}$ (d) over ASAB, (e) over DEBK and (f) Daily maximum (blue) and minimum (red) values of spatial gradient of TEC, in year 2014. The $ROTI_{ave}$ value in TECU/min is indicated in color code.

The maximum enhancement/reduction in the gradient of TEC observed during post-sunset and postmidnight period showing monthly and seasonal variations are the other features noticed from Figs. 5c and f. The maximum peak/reduced values of the spatial gradient of TEC observed in equinoctial months are greater than solstice months. Equinoctial asymmetry in the occurrence of TEC gradient was also noticed. TEC gradient in March equinox was greater than that in September equinox. The minimum values in the spatial gradient of TEC observed mostly during post-sunset and post-midnight periods show the same trend with that of the maximum enhancement in the gradient of TEC. They also show an equinoctial asymmetry, TEC gradient in March equinoxes were greater than the one obtained for September equinoxes.

Figures 5d and e present the daily maximum values of the phase fluctuation index ($ROTI_{ave}$) over ASAB and DEBK stations, respectively and Fig. 5f shows the daily maximum and minimum value of the gradient of TEC in the year 2014. It is clearly observed from the figures that the enhancement in $ROTI_{ave}$ and gradient of TEC shows monthly and seasonal

variations, and also equinoctial asymmetry is observed. The daily maximum value of the spatial gradient of TEC between the two stations shows similar trends with the daily maximum value of $ROTI_{ave}$ observed over ASAB and DEBK stations. The trend they show has similarity with the time of occurrence of maximum enhancement, monthly and seasonal variations. Moreover, the seasonal variation observed in both variables exhibits equinoctial asymmetry, where the March equinox was greater than September equinoxes. The mechanism of generation of the enhancement in vertical drift just after sunset was detailed by Farley et al. (2008). The magnitude of peak vertical drift is known to control the seasonal and day-to-day variations in the occurrence of equatorial spread F (Manju et al., 2009; Tulasi Ram et al., 2006).

Figure. 6 shows the relation between the spatial gradient of TEC and ROTI over ASAB and DEBK computed in the time period of 19:00-24:00 LT for geomagnetic quiet days of the year 2014. For every quiet day of the year 2014, an average of $\Delta TEC/\Delta lon$ and average of ROTI in the time period between 19:00 LT and 24:00 LT were computed. In this time period, a peak value in TEC gradient about 2.5 TECU/deg and ROTI about 1 TECU/min were observed. In the computation of TEC gradient, a positive and negative value in the TEC gradient were observed. The positive/negative in the TEC gradient means a maximum enhancement/reduced in the plasma density relative to each other. To analyze the effect of the horizontal gradient of TEC on navigation and communication during geomagnetic storms, Radicella et al. (2004) considered the absolute value of TEC gradient. Here, we took the absolute value of the spatial gradient of TEC to describe the relationship between the TEC gradient and ROTI. The correlation coefficient between $\Delta TEC/\Delta lon$ and ROTI is about 0.58 (in ASAB) and 0.53 (in DEBK), respectively. It is well known that ROT is the combination of the spatial and temporal gradients. However, by giving less attention to the spatial gradient effect, previous authors often use $\Delta TEC/\Delta t$ to explain the TEC fluctuation determination. It is not only the temporal variation of TEC that contribute to the fluctuation in the phase and amplitude of the signals but also the spatial gradient of TEC. The computed correlation coefficient between the TEC gradient and ROTI, here, gives an indication of the contribution of the spatial gradient of TEC to ROTI (or ROT) usage. This can give the case where the spatial gradient of TEC between two nearby located stations used as an indicator of occurrence of ionospheric irregularities. Cesaroni et al. (2015) described the importance of the information provided by the TEC gradients variability and the role of the meridional TEC gradients in driving scintillation. By comparing the zonal and the meridional components of average and standard deviation of ΔTEC, Cesaroni et al. (2015) reported that the North-South (N-S) gradients of TEC are significantly larger than their East-West (E-W) counterparts, regardless of the season. Saito and Yoshihara (2017) associated extreme ionospheric total electron gradient with plasma bubbles for GNSS Ground-Based Augmentation System and they obtained a largest ionospheric gradient of about 3.38 TECU/km.

Figure 7 presents the percentage occurrence of ionospheric irregularities over ASAB (blue) and DEBK (red) in the year 2014. The observation of this percentage occurrence is for all days of the year 2014 including both quiet and disturbed periods. The percentage occurrence of irregularities was calculated by counting the number of days in a month with $ROTI_{ave} \geq 0.4$ TECU/min and dividing by the number of days in a month for which data are available, and multiplied by 100 $\%$ (Oladipo et al., 2014). The two peaks of irregularity occurrence were observed around the middle of the equinoxes (i.e., in March and September) at both stations. This could be related to the alignment of the magnetic field lines with a geographic meridian (Burke

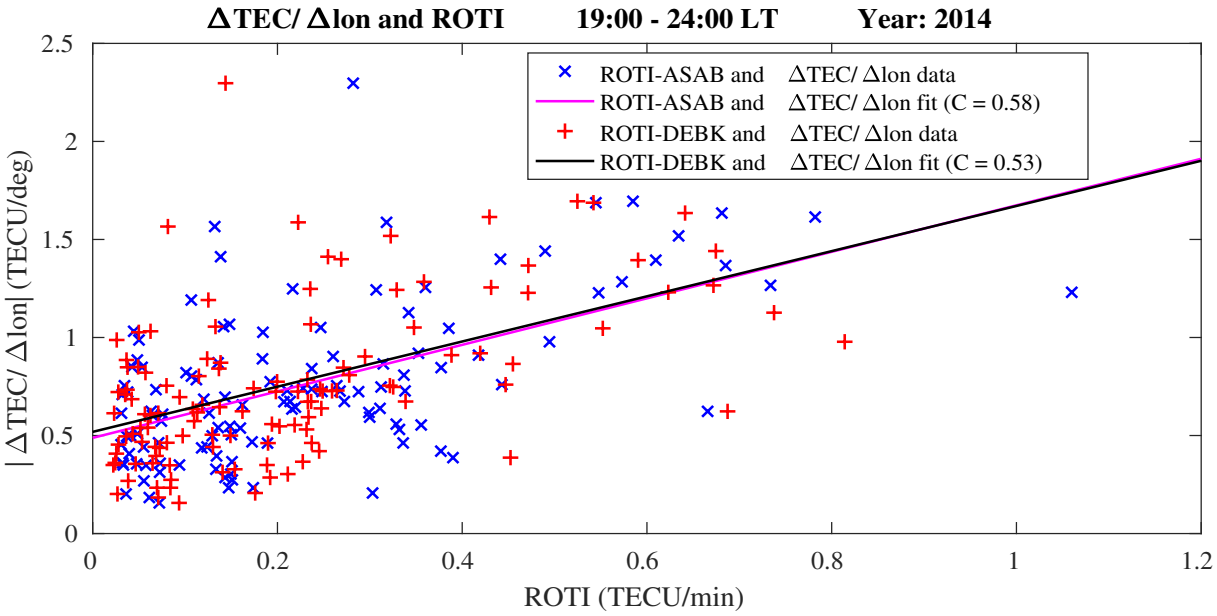

Figure 6. Relation between the spatial gradient of TEC and ROTI index derived from TEC over ASAB (blue) and DEBK (red) during 19:00-24:00 LT period of the magnetic quiet days of year 2014. The black and magnta lines indicate the linear fit between the spatial gradient of TEC and ROTI for ASAB and DEBK, respectively.

et al., 2004; Tsunoda, 2005, 2010). The seasonal variation of ionospheric irregularities exhibits an equinoctial asymmetry in its occurrence especially at the two peaks (i.e., in March and September), where March equinox is greater than that of September equinox. The maximum $ROTI_{ave}$ observed over this station in the year 2014 was about 1.8 TECU/min in March 2014. It is evident from the figure that the minimum level of $ROTI_{ave}$ was observed on December Solstice. Based on a few station observations, earlier studies indicated that equinoctial asymmetry in the occurrence of L-band scintillations may be attributed to differences in the meridional winds during two equinoxes (e.g., Nishioka et al., 2008; Maruyama et al., 2006; Otsuka et al., 2006). Nishioka et al. (2008) have shown the occurrence characteristics of plasma bubbles using GPS-TEC obtained all over the globe and found equinoctial asymmetry in the occurrence of plasma bubbles. They have suggested that equinoctial asymmetry could be due to the asymmetric distribution of integrated conductivities during these equinoctial periods. Using three ionosondes observations, Maruyama et al. (2006) reported that meridional wind is the key factor for the equinoctial asymmetry. Using multi-instrument observations, Sripathi et al. (2011) examined the equinoctial asymmetry in scintillation occurrence in the Indian sector and proposed the asymmetry in the electron density distribution and meridional winds as a possible causative mechanism. Manju et al. (2012) also reported equinoctial asymmetry in ESF occurrence and discussed the possible role of asymmetric meridional winds. Dasgupta et al. (1983) studied the equinoctial asymmetry in equatorial and low latitude F region ionization distribution and attributed it to neutral composition changes. Manju and Haridas (2015) observed a significant asymmetry in the threshold height between the vernal equinox and autumn equinox and underlines the distinct

differences in the role of neural dynamics in ESF triggering during the two equinoxes. The local time and seasonal trends of occurrence of ionospheric irregularities observed in this study are similar to those reported in the previous studies (Aarons, 1993; Basu et al., 1988; Olwendo et al., 2013; Amabayo et al., 2014; Seba and Tsegaye, 2015). Based on scintillation index (S_4) and GPS-TEC derived indices, Susnik and Forte (2011), Paznukhov et al. (2012), Oladipo and Schuler (2013b), Oladipo et al. (2014), Seba and Tsegaye (2015) and Mungufeni et al. (2016) reported the seasonal and equinoctial asymmetry in the occurrence of ionospheric irregularities over equatorial/low-latitude region of African.

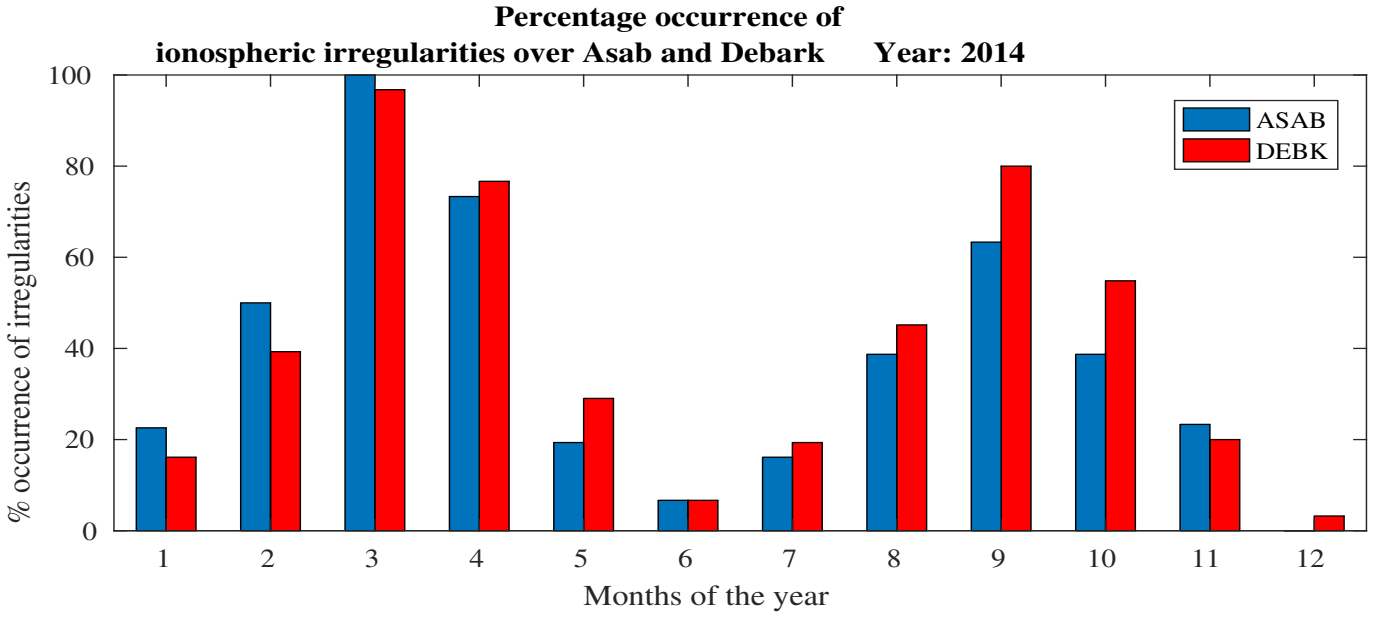

Figure 7. Percentage of occurrence of ionospheric irregularities over ASAB (red) and DEBK (blue) stations in the year 2014 based on $ROTI_{ave}$ index.

In terms of local time, monthly, and seasonal behavior the enhancement/reduction in the spatial gradient of TEC and occurrence of ionospheric irregularities show similar trends. And, it is evident from the above result that the spatial gradient of TEC between two nearby located stations where the two receivers lie nearly along the same latitudes could be used as an indicator of the occurrence of large-scale ionospheric irregularities. In the current study, the optimum distance between the two GNSS receivers and the threshold value of the gradient of TEC that could indicate the occurrence of ionospheric irregularities has not been considered. This will be done in our future work.

4 Conclusions

In this study, we present the possibility that the spatial gradient of TEC between two nearby located stations (ASAB and DEBK) over East Africa the longitudinal sector could be used as an indicator of the occurrence of large-scale ionospheric

irregularities. The following features were observed in the study. Most of the daily maximum enhancement and reduction of the spatial gradient of TEC was observed in the pre-midnight and post-midnight period. In terms of seasons, months and local times, the maximum enhancement/reduction in the spatial gradient of TEC and $ROTI_{ave}$ show similar tends. Both of them show maximum enhancement/reduction during the months of March and September equinoxes. Equinoctial asymmetry both in the spatial gradient and in the ROT was also observed, where March equinox was greater than September equinox. Peak values in the spatial gradient of TEC and $ROTI_{ave}$ were observed about 1-2 hrs later from post-sunset enhancement of equatorial electric field (EEF). The correlation coefficient between the magnitude of the spatial gradient of TEC and ROTI was about 0.58 (in ASAB station) and 0.53 (in DEBK station). Based on the above results, the spatial gradient of TEC between the two nearby located stations lying along the same geographic and geomagnetic latitudes could be used as an indicator of the occurrence of large-scale ionospheric irregularities. The spatial gradient of electron density (TEC) near solar-terminator obtained from two nearby located GNSS receivers method may be an alternative method to estimate the strength of the zonal electric field. The threshold value of the gradient of TEC and the minimum separation distance between stations were not presented in the current study and this will be considered in the future investigation.

Acknowledgments

We thank Ethiopian Space Science and Technology Institute (ESSTI) for facilitating conditions to do this research. We also acknowledge the administration and staff the Space Science Directorate of the South African National Space Agency (SANSA) for the support during the research visit of the first author to the institution. The authors would like to express their gratitude to the International GNSS Service (IGS) for providing the GPS data (ftp://cddis.gsfc.nasa.gov). We thank the Cooperative Institute for Research in Environmental Sciences (CIRES) team for real-time PPEEFM model at http://geomag.org/model/PPEFM/RealtimeEF.html. We are also grateful to the online AMBER (http://magnetometers.bc.edu/index.php/) and INTERMAGNET (http://www.intermagnet.org/) for freely providing magnetometer data. Melessew Nigussie work has been supported by Air Force Office of Scientific Research, Air Force Material Command USAF under Award No.FA9550-16-1-0070. T. Dugassa, thanks Bule Hora University for permitting study leave.

Data availability

The data used in this study were obtained from ftp://cddis.gsfc.nasa.gov, http://geomag.org/models/PPEFM/RealtimeEF.html, http://magnetometers.bc.edu/index.php/, http://www.intermagnet.org/, and http://isgi.unistra.fr/data_download.php.

Competing interests

The authors declare that they have no conflict of interest.

References

Aarons, J.: The longitudinal morphology of equatorial F layer irregularities relevant to their occurrence., Space Sci. Rev., 63, 209., 1993.

Aarons, J., Mendillo, M., and Yantosca, R. G.: GPS phase fluctuations in the equatorial region during sunspot minimum., Radio Sci.., 32, 1535-1550., 1997.

Abadi, P., Otsuka, Y., and Tsugawa, T.: Effects of pre-reversal enhancement of E× B drift on the latitudinal extension of plasma bubble in Southeast Asia, Earth, Planets and Space, 67, 74, 2015.

Abdu, M. A., . Batista, I. S., Reinisch, B. W., de Souza, J. R., Sobral, J. H. A., Pedersen, T. R., Medeiros, A. F., Schuch, N. J., and de Paula, E. R., a. G. K. M.: Conjugate Point Equatorial Experiment (COPEX) campaign in Brazil: Electrodynamics highlights on spread development conditions and day to day variablity, J. Geophys. Res., 114, A04308, https://doi.org/10.1029/2008JA013749, 2009.

Ajith, K., Tulasi Ram, S., Yamamoto, M., Otsuka, Y., and Niranjan, K.: On the fresh development of equatorial plasma bubbles around the midnight hours of June solstice, Journal of Geophysical Research: Space Physics, 121, 9051–9062, 2016.

Amabayo, E., Jurua, E., Cilliers, P., and Habarulema, J.: Climatology of ionospheric scintillations and TEC trend over the Ugandan region. , Adv. Space Res., 53,734-743., 2014.

Anderson, D., Anghel, A., Yumoto, K., Ishitsuka, M., and Kudeki, E.: Estimating daytime vertical $E \times B$ drift velocities in the equatorial F-region using ground-based magnetometer observations, Geophys. Res. Lett., 29(12), 1596, https://doi.org/10.1029/2001GL014562, 2002.

Anderson, D., Anghel, A., Chau, J., and Veliz, O.: Daytime vertical E× B drift velocities inferred from ground-based magnetometer observations at low latitudes, Space Weather, 2, 2004.

Anderson, D., Anghel, A., Chau, J. L., and Yumoto, K.: Global, low-latitude, vertical E× B drift velocities inferred from daytime magnetometer observations, Space Weather, 4, 2006.

Arikan, F., Nayir, H., Sezen, U., and Arikan, O.: Estimation of single station interfrequency receiver bias using GPS-TEC, Radio Science, 43, 2008.

Basu, S. and Basu, S.: Equatorial scintillations-A review, Journal of Atmospheric and Terrestrial Physics, 43, 473–489, 1981.

Basu, S., MacKenzie, E., and Basu, S.: Ionospheric constraints on VHF/UHF communications links during solar maximum and minimum periods, Radio Science, 23, 363–378, 1988.

Basu, S., Kudeki, E., Basu, S., Valladares, C., Weber, E., Zengingonul, H., Bhattacharyya, S., Sheehan, R., Meriwether, J., Biondi, M., Kuenzler, H., and Espinoza, J.: Scintillations, plasma drifts, and neutral winds in the equatorial ionosphere after sunset, J. Geophys Res, 101, 26795-26809, 1996.

Bhattacharyya, A., Beach, T., Basu, S., and Kintner, P.: Nighttime equatorial ionosphere: GPS scintillations and differential carrier phase fluctuations, Radio Science, 35, 209–224, 2000.

Bolaji, O., Adebiyi, S., and Fashae, J.: Characterization of ionospheric irregularities at different longitudes during quiet and disturbed geomagnetic conditions, Journal of Atmospheric and Solar-Terrestrial Physics, 182, 93–100, 2019.

Burke, W. J., Gentile, L. C., Huang, C. Y., Valladares, C. E., and Su, S. Y.: Longitudinal variability of equatorial plasma bubbles observed by DMSP and ROCSAT-1, J. Geophys. Res., 19, https://doi.org/10.1029/2004JA010583, 2004.

Cesaroni, C., Spogli, L., Alfonsi, L., De Franceschi, G., Ciraolo, L., Monico, J. F. G., Scotto, C., Romano, V., Aquino, M., and Bougard, B.: L-band scintillations and calibrated total electron content gradients over Brazil during the last solar maximum, Journal of Space Weather and Space Climate, 5, A36, 2015.

Chu, F., Liu, J.Y., a. T. H., Sobral, J., Taylor, M., and Medeiros, A. F.: The climatology of ionospheric plasma bubbles and irregularities over Brazil, Annales Geophysical, 23: 379-384, 2005.

Crain, D., Heelis, R., and Bailey, G.: Effects of electrical coupling on equatorial ionospheric plasma motions: When is the F region a dominant driver in the low-latitude dynamo?, Journal of Geophysical Research: Space Physics, 98, 6033–6037, 1993.

Dabas, R., Singh, L., Lakshmi, D., Subramanyam, P., Chopra, P., and Garg, S.: Evolution and dynamics of equatorial plasma bubbles: Relationships to ExB drift, postsunset total electron content enhancements, and equatorial electrojet strength, Radio Science, 38, 2003.

Dasgupta, A., Anderson, D., and Klobuchar, J.: Equatorial F-region ionization differences between March and September, Adv. Space Res., 10, 199-202, 1983.

Dugassa, T., Habarulema, J. B., and Nigussie, M.: Longitudinal variability of occurrence of ionospheric irregularities over the American, African and Indian regions during geomagnetic storms, Advances in Space Research, 2019.

Echer, E., Tsurutani, B., and Gonzalez, W.: Interplanetary origins of moderate (- 100 nT< Dst- 50 nT) geomagnetic storms during solar cycle 23 (1996–2008), Journal of Geophysical Research: Space Physics, 118, 385–392, 2013.

Farley, D., Balsey, B., Woodman, R., and McClure, J.: Equatorial spread F: Implications of VHF radar observations, Journal of Geophysical Research, 75, 7199–7216, 1970.

Farley, D. T., Bonelli, E., Fejer, B. G., and Larsen, M. F.: The prereversal enhancement of the zonal electric field in the equatorial ionosphere., J. Geophys. Res., 113,A05304., 2008.

Fejer, B.: Low latitude electrodynamics plasma drifts: a review., J. Atmos. Terr. Phys., 53, 677-693, 1991.

Fejer, B., Jensen, J., and Su, S.: Quiet time equatorial F region vertical plasma drift model derived from ROCSAT-1 observations., J. Geophys. Res., https://doi.org/http://dx.doi.org/10.1029/2007JA012801., 2008.

Fejer, B. G.: Low latitude ionospheric electrodynamics, Space Science Reviews, 158, 145–166, 2011.

Fejer, B. G., Scherliess, L., and de Paula, E. R.: Effects of the vertical plasma drift velocity on the generation and evolution of equatorial spread F, J. Geophys. Res., 104, 19,859-19,869, https://doi.org/10.1029/1999JA900271, 1999.

Hajra, R., Chakraborty, S., Mazumdar, S., and Alex, S.: Evolution of equatorial irregularities under varying electrodynamical conditions: a multitechnique case study from Indian longitude zone, Journal of Geophysical Research: Space Physics, 117, 2012.

Horvath, I. and Essex, E.: Vertical E$\times$ B drift velocity variations and associated low-latitude ionospheric irregularities investigated with the TOPEX and GPS satellite data, in: Annales Geophysicae, vol. 21, pp. 1017–1030, 2003.

Jakowski, N., Leitinger, R., and Ciraolo, L.: Behaviour of large scale structures of the electron content as a key parameterfor range errors in GNSS applications, Annals of Geophysics, 47, 2004.

Jakowski, N., Stankov, S., and Klaehn, D.: Operational space weather service for GNSS precise positioning, in: Annales Geophysicae, vol. 23, pp. 3071–3079, 2005.

Kassa, T. and Damtie, B.: Ionospheric irregularities over Bahir Dar, Ethiopia during selected geomagnetic storms, Advances in Space Research, 60, 121–129, 2017.

Kelley, M. C.: The Earth's ionosphere: plasma physics and electrodynamics, vol. 96, Academic press, 2009.

Ma, G. and Maruyama, T.: Derivation of TEC and estimation of instrumental biases from GEONET in Japan, in: Annales Geophysicae, vol. 21, pp. 2083–2093, 2003.

Ma, G. and Maruyama, T.: A super bubble detected by dense GPS network at East Asian longitudes., Geophys. Res. Lett., 133, L21103, 2006.

Magdaleno, S., Herraiz, M., Altadill, D., and Benito, A.: Climatology characterization of equatorial plasma bubbles using GPS data, Journal of Space Weather and Space Climate, 7, A3, 2017.

Manju, G. and Haridas, M. M.: On the equinoctial asymmetry in the threshold height for the occurrence of equatorial spread F, Journal of Atmospheric and Solar-Terrestrial Physics, 124, 59–62, 2015.

Manju, G., Devasia, C., and Ravindran, S.: The seasonal and solar cycle variations of electron density gradient scale length, vertical drift and layer height during magnetically quiet days: Implications for Spread F over Trivandrum, India, Earth, planets and space, 61, 1339–1343, 2009.

Manju, G., Haridas, M., Ravindran, S., Pant, T. K., and Ram, S. T.: Equinoctial asymmetry in the occurrence of equatorial spread-F over Indian longitudes during moderate to low solar activity period 2004-2007, 94.20. dt; 94.20. Vv; 96.60. qd, 2012.

Manoj, C. and Maus, S.: A real-time forecast service for the ionospheric equatorial zonal electric field., Space Weather, 10, https://doi.org/http://dx.doi.org/10.1029/2012SW00082, 2012.

Martinis, C. R., Mendillo, M. J., and Aarons, J.: Toward a synthesis of equatorial spread F onset and suppression during geomagnetic storms, J. Geophys. Res., 110, A07306, https://doi.org/10.1029/2003JA010362, 2005.

Maruyama, T., Saito, S., Kawamura, M., Nozaki, K., Krall, J., and D.Huba, J.: Equinoctial asymmetry of a low-latitude ionosphere-thermosphere system and equatorial irregularities: Evidence for meridional wind control., Ann. Geophys., 27, 2027-2034, https://doi.org/10.5194/angeo-27-2027-2009, 2006.

Mendillo, M., Lin, B., and Aarons, J.: The application of GPS observations to equatorial aeronomy., Radio Sci., 35, 885-904., 2000.

Mendillo, M., Meriwether, J., and Biondi, M.: Testing the thermospheric neutral wind suppression mechanism for day-to-day variability of equatorial spread F., J. Geophys. Res., 106, 3655., 2001.

Muella, M., De Paula, E., Kantor, I., Batista, I., Sobral, J., Abdu, M., Kintner, P., Groves, K., and Smorigo, P.: GPS L-band scintillations and ionospheric irregularity zonal drifts inferred at equatorial and low-latitude regions, Journal of Atmospheric and Solar-Terrestrial Physics, 70, 1261–1272, 2008.

Mungufeni, P., Jurua, E., and Habarulema, J.: Trends of ionospheric irregularities over African low latitude region during quiet geomagnetic conditions., J. Atmos. Solar Terr. Phys., 138-139, 261-267, https://doi.org/http://dx.doi.org/10.1016/j.jastp.2016.01.015, 2016.

Mushini, S. C., P. T. J. R. B. L. J. W. M. and Pokhotelov, D.: Improved amplitude and phase scintillation indices derived from wavelet detrended high latitude GPS data, PS Solut., https://doi.org/10.1007/s10291-011-0238-4, 2011.

Nava, B., Radicella, S., Leitinger, R., and Coïsson, P.: Use of total electron content data to analyze ionosphere electron density gradients, Advances in Space Research, 39, 1292–1297, 2007.

Nayak, C., Tsai, L.-C., Su, S.-Y., Galkin, I., Caton, R., and Groves, K.: Suppression of ionospheric scintillation during St. Patrick's Day geomagnetic super storm as observed over the anomaly crest region station Pingtung, Taiwan: A case study, Advances in Space Research, 60, 396-405, https://doi.org/http://dx.doi.org/10.1016/j.asr.2016.11.036, 2017.

Nishioka, M., Saito, A., and Tsugawa, T.: Occurrence characteristics of plasma bubble derived from global ground-based GPS receiver networks, J. Geophys. Res., 113, A05301, https://doi.org/10.1029/2007JA012605, 2008.

Oladipo, O. A. and Schuler, T.: Magnetic storm effect on the occurrence of ionospheric irregularities at an equatorial station in the African sector, Ann.Geophys., 56, 5, A0565, https://doi.org/10.4401/ag-6247, 2013a.

Oladipo, O. A. and Schuler, T.: Equatorial ionospheric irregularities using GPS TEC derived index., Atmos. Sol. Terr. Phys., 92, 78-82., 2013b.

Oladipo, O. A., Adeniyi, J. O., Olawepo, A. O., and Doherty, P. H.: Large-scale ionospheric irregularities occurrence at Ilorin, Nigeria, Space Weather., 12, 300-305., https://doi.org/10.1002/2013SW000991, 2014.

Olwendo, O., Baluku, T., Baki, P., Cilliers, P., Mito, C., and Doherty, P.: Low latitude ionospheric scintillation and zonal irregularity drifts observed with GPS-SCINDA system and closely spaced VHF receivers in Kenya, Adv. in Space Res., 51, 1715-1726., https://doi.org/http://dx.doi.org/10.1016/j.asr.2012.12.017, 2013.

Otsuka, Y., Shiokawa, K., and Ogawa, T.: Equatorial ionospheric scintillations and zonal irregularity drifts observed with closely spaced GPS receivers in Indonesia., J. Meteorol. Soc. Jpn., 84A, 343-351, 2006.

Otsuka, Y., Ogawa, T., et al.: VHF radar observations of nighttime F-region field-aligned irregularities over Kototabang, Indonesia, Earth, planets and space, 61, 431–437, 2009.

Paznukhov, V., Carrano, C., Doherty, P., Groves, K., Caton, R.G., a. V. C., Seemala, G., Bridgwood, C., Adeniyi, J., Amaeshi, L., Damtie, B., a. D. M. F., Ndeda, J., Baki, P., Obrou, O., Okere, B., and Tsidu, G.: Equatorial plasma bubbles and L-band scintillations in Africa during solar minimum., Ann. Geophys., 30, 675-682, 2012.

Pi, X., Mannucci, A. J., Lindqdwister, U. J., and Ho, C.: Monitoring of Global Ionospheric Irregularities using the worldwide GPS, Geophys. Res. Lett., 24, 2283-2286, https://doi.org/10.1029/97GL02273, 1997.

Radicella, S. M., Nava, B., Coïsson, P., Kersley, L., and Bailey, G. J.: Effects of gradients of the electron density on Earth-space communications, Annals of Geophysics, 47, 2004.

Ram, S. T., Rao, P. R., Prasad, D., Niranjan, K., Babu, A. R., Sridharan, R., Devasia, C., and Ravindran, S.: The combined effects of electrojet strength and the geomagnetic activity (Kp-index) on the post sunset height rise of the F-layer and its role in the generation of ESF during high and low solar activity periods, Ann. Geophys, 25, 2007.

Rao, P. R., Krishna, S. G., Niranjan, K., and Prasad, D.: Study of spatial and temporal characteristics of L-band scintillations over the Indian low-latitude region and their possible effects on GPS navigation, in: Annales Geophysicae, vol. 24, pp. 1567–1580, 2006a.

Rao, P. R., Krishna, S. G., Niranjan, K., and Prasad, D.: Temporal and spatial variations in TEC using simultaneous measurements from the Indian GPS network of receivers during the low solar activity period of 2004-2005, in: Annales Geophysicae, vol. 24, pp. 3279–3292, 2006b.

Rastogi, R. and Woodman, R.: Spread F in equatorial ionograms associated with reversal of horizontal F region electric field, in: Annales de Geophysique, vol. 34, pp. 31–36, 1978.

Rastogi, R., Kitamura, T., and Kitamura, K.: Geomagnetic field variations at the equatorial electrojet station in Sri Lanka, Peredinia, in: Annales Geophysicae, vol. 22, pp. 2729–2739, 2004.

Rastogi, R. G. and Klobuchar, J. A.: Ionospheric electron content within the equatorial F2 layer anomaly belt., J. Geophys. Res, 95(A11),19,045-19,052, 1990.

Ravi Chandra, K., Satya Srinivas, V., and Sarma, A.: Investigation of ionospheric gradients for GAGAN application, Earth, planets and space, 61, 633–635, 2009.

Ray, S., Paul, A., and Dasgupta, A.: Equatorial scintillations in relation to the development of ionization anomaly, in: Annales Geophysicae, vol. 24, pp. 1429–1442, 2006.

Rungraengwajiake, S., Supnithi, P., Saito, S., Siansawasdi, N., and Saekow, A.: Ionospheric delay gradient monitoring for GBAS by GPS stations near Suvarnabhumi airport, Thailand, Radio Science, 50, 1076–1085, 2015.

Saito, S. and Yoshihara, T.: Evaluation of extreme ionospheric total electron content gradient associated with plasma bubbles for GNSS Ground-Based Augmentation System, Radio Science, 52, 951-962, 2017.

Sardón, E. and Zarraoa, N.: Estimation of total electron content using GPS data: How stable are the differential satellite and receiver instrumental biases?, Radio science, 32, 1899–1910, 1997.

Seba, E. and Tsegaye, K. G.: Characterization of ionospheric scintillation at a geomagnetic equatorial region station., Adv. Space Res., 56, 2057-2063, 2015.

Seba, E. B., Nigussie, M., and Moldwin, M. B.: The relationship between equatorial ionization anomaly and nighttime equatorial spread F in East Africa, Advances in Space Research, 62, 1737–1752, 2018.

Seemala, G. and Valladares, C.: Statistics of total electron content depletions observed over the South American continent for the year 2008, Radio Science, 46, RS5019, 2011.

Sreeja, V., Devasia, C., Ravindran, S., and Pant, T. K.: Observational evidence for the plausible linkage of Equatorial Electrojet (EEJ) electric field variations with the post sunset F-region electrodynamics, in: Annales geophysicae: atmospheres, hydrospheres and space sciences, vol. 27, p. 4229, 2009.

Sripathi, S., Kakad, B., and Bhattacharyya, A.: Study of equinoctial asymmetry in the Equatorial Spread F (ESF) irregularities over Indian region using multi-instrument observations in the descending phase of solar cycle 23, J. Geophys. Res., 116, A11302, https://doi.org/10.1029/2011JA016625., 2011.

Susnik, A. and Forte, B.: Ionospheric scitillation activity measured in the African sector, paper presented at General Assembly and Scientific Symposium, XXXth URSI, Istanbul, Turkey., 2011.

Tsunoda, R.: Control of the seasonal and longitudinal occurrence of equatorial scintillations by the longitudinal gradient in integrated E region Pederson conductivity., J. Geophys. Res., 90, 447., 1985.

Tsunoda, R. T.: On the enigma of day-to-day variability in Wave structure in equatorial Spread F, Geophys. Res. Lett., 32, 2005.

Tsunoda, R. T.: On seeding equatorial spread F during solstices, Geophys. Res. Lett., 37, L05102., https://doi.org/http://dx.doi.org/10.1029/2010GL042576., 2010.

Tulasi Ram, S., Rao, P. V. S. R., Niranjan, K., Prasad, D. S. V. V. D., Sridharan, R., Devasia, C. V., and Ravindran, S.: The role of post-sunset vertical drifts at the equator in predicting the onset of VHF scintillations during high and low sunspot activity years., Ann. Geophys., 24, 1609-1616, 2006.

Uemoto, J., Maruyama, T., Saito, S., Ishii, M., and Yoshimura, R.: Relationships between pre-sunset electrojet strength, pre-reversal enhancement and equatorial spread-F onset., Annales Geophysicae (09927689), 28, 2010.

Valladares, C., Basu, S., Groves, K., Hagan, M., Hysell, D., Mazzella Jr., A., and Sheehan, R.: Measurement of the latitudinal distribution of total electron content during equatorial spread-F events, J. Geophys. Res., 106, 29133-29152, 2001.

Valladares, C., Villalobos, J., Sheehan, R., and Hagan, M.: Latitudinal extension of low-latitude scintillations measured with a network of GPS receivers, Ann. Geophys., 22, 3155-3175, 2004.

Watthanasangmechai, K., Yamamoto, M., Saito, A., Tsunoda, R., Yokoyama, T., Supnithi, P., Ishii, M., and Yatini, C.: Predawn plasma bubble cluster observed in Southeast Asia, Journal of Geophysical Research: Space Physics, 121, 5868–5879, 2016.

Wernik, A. and Liu, C.: Ionospheric irregularities causing scintillation of GHz frequency radio signals, Journal of Atmospheric and Terrestrial Physics, 36, 871–879, 1974.

Wiens, R. H., Ledvina, B. M., a. K. P. M., Afewerki, M., and Mulugheta, Z.: Equatorial plasma bubbles in the ionosphere over Eritrea: Occurrence and drift speed, Ann. Geophys.,, 24, 1443–1453, 2006.

Woodman, R.: Vertical drift velocities and East-West electric fields at the magnetic equator., J. Geophys. Res., 75(31), 6249-6259, https://doi.org/10.1029/JA075i031p06249, 1970.

Yizengaw, E. and Moldwin, M. B.: African Meridian B-field Education and Research (AMBER) array., Earth Moon Planet, 104, 237-246, https://doi.org/10.1007/s11038-008-9287-2, 2009.

Yizengaw, E., Moldwin, M. B., Mebrahtu, A., Damtie, B., Zesta, E., Valladares, C. E., and Doherty, P.: Comparison of storm time equatorial ionospheric electrodynamics in the African and American sectors, J. Atmos. Sol.-Terr. Phys., 73(1), 156–163, https://doi.org/10.1016/j.jastp.2010.08.008., 2011.

Yizengaw, E., Zesta, E., a. M. M. B., Damtie, B., Mebrahtu, A., Valladares, C. E., and Pfaff, R. F.: Longitudinal differences of ionospheric vertical density distribution and equatorial electrodynamics., J. Geophys. Res., 117, A07312, https://doi.org/10.1029/2011JA017454., 2012.

Yizengaw, E., Moldwin, M. B., Zesta, E.and Biouele, C. M., Damtie, B., Mebrahtu, A., Rabiu, B., Valladares, C. F., and Stoneback, R.: The longitudinal variability of equatorial electrojet and vertical drift velocity in the African and American sectors., Ann. Geophys., 32, 231-238, 2014.